PATZ1 Is a DNA Damage-Responsive Transcription Factor That Inhibits p53 Function

Nazli Keskin,[a,b] Emre Deniz,[a,b] Jitka Eryilmaz,[a*] Manolya Un,[a] Tugce Batur,[a] Tulin Ersahin,[c,d] Rengul Cetin Atalay,[c,d] Shinya Sakaguchi,[e] Wilfried Ellmeier,[e] Batu Erman[a,b]

Biological Sciences and Bioengineering Program, Faculty of Engineering and Natural Sciences, Sabanci University, Istanbul, Turkey[a]; Sabanci University Nanotechnology Research and Application Center-SUNUM, Istanbul, Turkey[b]; Department of Molecular Biology and Genetics, Bilkent University, Ankara, Turkey[c]; Informatics Institute, Middle East Technical University, Ankara, Turkey[d]; Division of Immunobiology, Institute of Immunology, Center for Pathophysiology, Infectiology and Immunology, Medical University of Vienna, Vienna, Austria[e]

Insults to cellular health cause p53 protein accumulation, and loss of p53 function leads to tumorigenesis. Thus, p53 has to be tightly controlled. Here we report that the BTB/POZ domain transcription factor PATZ1 (MAZR), previously known for its transcriptional suppressor functions in T lymphocytes, is a crucial regulator of p53. The novel role of PATZ1 as an inhibitor of the p53 protein marks its gene as a proto-oncogene. PATZ1-deficient cells have reduced proliferative capacity, which we assessed by transcriptome sequencing (RNA-Seq) and real-time cell growth rate analysis. PATZ1 modifies the expression of p53 target genes associated with cell proliferation gene ontology terms. Moreover, PATZ1 regulates several genes involved in cellular adhesion and morphogenesis. Significantly, treatment with the DNA damage-inducing drug doxorubicin results in the loss of the PATZ1 transcription factor as p53 accumulates. We find that PATZ1 binds to p53 and inhibits p53-dependent transcription activation. We examine the mechanism of this functional inhibitory interaction and demonstrate that PATZ1 excludes p53 from DNA binding. This study documents PATZ1 as a novel player in the p53 pathway.

Wild-type (WT) p53 is a stress-responsive, sequence-specific transcription factor that inhibits the cell cycle, promotes senescence, and, if the insult to cellular health is not resolved, induces apoptotic death (1). p53 mutations that allow cells to escape this death are the most common genetic event in human cancer (2). Alternative mechanisms of escape rely on the overexpression of MDM2 and MDMX, major negative regulators of p53 that keep p53 levels low under unstressed conditions through ubiquitination-mediated degradation (3). Moreover, many DNA tumor viruses encode proteins that can inactivate p53 (2). However, the list of p53 regulators is far from complete. Various stress conditions result in the upregulation of p53, controlled by feedback loops, posttranslational modifications, and epigenetic changes. In the present study, we aimed to find new players that modify p53 function.

p53 is composed of an N-terminal transactivation domain (through which it interacts with MDM2), a proline-rich domain, central DNA binding and tetramerization domains, and a C-terminal regulatory domain. p53 binds response elements (REs) in nuclear DNA, which results in stress-induced changes (either up- or downregulation) in gene expression. Tetrameric p53 binds REs that are composed of two half-sites, each with a consensus of RR RCWWGYYY, separated by 0 to 21 bases (where R is a purine, Y is a pyrimidine, and W is either an A or T) (4). p53 REs can be subcategorized as those that respond to low levels of wild-type p53, those that respond to stabilized p53 after stress, and those that respond to p53 with mutations in its DNA binding domain. A recent study found 160 p53 REs controlling 129 genes in the human genome (5). Another study using chromatin immunoprecipitation (ChIP) with paired-end ditag (PET) sequencing identified 542 functional p53 binding sites in the human genome (6). Similarly, a study using ChIP followed by RNA sequencing (ChIP-Seq) found that 3,697 target genes were bound and differentially regulated by p53 in doxorubicin (DOX) (Adriamycin)-treated

mouse embryonic stem cells (7). Yet another ChIP-Seq study revealed that of the 3,193 genes with nearby p53 REs, 432 were regulated by DOX in mouse embryonic fibroblasts (MEFs) (8).

In the present study, we have identified the role of a BTB-ZF (broad-complex, tramtrack, and bric-à-brac zinc finger) transcription factor, PATZ1 (POZ-AT hook-zinc finger) that inhibits the ability of p53 to bind to its REs. PATZ1 has an N-terminal BTB domain for protein interaction, a central DNA binding AT hook domain, and a second, C-terminal, zinc finger (ZF) DNA binding domain (9–11). A recent ChIP-Seq study identified that the PATZ1 binding consensus can be either AT rich or GC rich (12). The specificity for two different consensus sequences is likely due to two different (AT hook and ZF) DNA binding domains.

Members of the BTB-ZF transcription factor family control diverse yet potentially related processes in cancer, development, and stem cell biology. PATZ1 can interact with other BTB-ZF transcription factors such as BCL-6 and Bach to control important cell fate decisions (13, 14). While PATZ1 was originally identified as a lymphocyte specific c-Myc-regulating transcription factor, its

expression and function are not restricted only to T lymphocytes ([15–19]). Early embryonic expression is likely functional, as $Patz1^{-/-}$ mice are born at a non-Mendelian frequency and are small in size ([16], [17]). PATZ1 is expressed in human colon and testicular cancer cell lines and is deleted or translocated to the Ewing sarcoma gene (*EWS*) in small-cell sarcoma ([9], [17], [20]). The PATZ1 protein was recently shown to be an inhibitor of p53-dependent endothelial cell senescence and was also shown to interact with p53 ([17], [21]).

We undertook the present study to identify factors that control p53 function. We used state-of-the-art techniques such as transcriptome sequencing (RNA-Seq) and real-time cell growth experiments to show that PATZ1 promotes cellular proliferation. We discovered that PATZ1 is regulated by DNA damage and can bind to and inhibit the transcriptional activity of p53. We characterized the interaction of p53 with PATZ1 and its alternatively spliced variants. We found that at least one of the four known *Patz1* gene products binds to p53 and interferes with p53 function by preventing p53 DNA binding. Even though previous studies on PATZ1 focused on its role in T lymphocytes, we discovered the global and unbiased effects of its absence on cell proliferation, adhesion, and morphology. Collectively, our findings indicate that PATZ1 is a novel regulator of p53-dependent transcription.

MATERIALS AND METHODS

Generation of MEFs. WT and $Patz1^{-/-}$ MEFs were isolated from 13.5-day-old embryos and analyzed at early (<5) passages. All mice were bred and maintained in the animal facility of the Medical University of Vienna, and animal experiments were done according to protocols approved by the Austrian Federal Ministry for Education, Science, and Art.

Cell lines, transfections, gene transfer, and treatment. HCT116, HCT116 p53$^{-/-}$, HEK293T, HeLa, NIH 3T3, AKR1, EL4, 3B4.14 T-hybridoma, RLM11 (a radiation-induced BALB/c thymoma cell line) ([22]), and VL3.3M2 DP thymocyte (a gift from C. Guidos) ([23]) cell lines were cultured in Dulbecco's modified Eagle's medium (DMEM) or RPMI 1640 supplemented with 10% fetal bovine serum and 50 μg/ml each of penicillin and streptomycin. HCT116 and HCT116 p53$^{-/-}$ cells were transfected by using polyethylenimine (PEI) (catalog number 23966; Polysciences Inc.) with a 3:1 (wt/wt) ratio of PEI to total DNA. The appropriate amounts of plasmid DNA were diluted in serum-free DMEM followed by PEI and vortexed immediately. The mix was incubated for 15 min at room temperature and added dropwise onto cells that were split 1 day before transfection. Lysis for Western blotting or luciferase assays was performed 48 h after transfection.

Human HCT116 cells were made susceptible to retroviral infection by transient transfection with a cDNA encoding the mouse cationic amino acid transporter (mCAT) (Addgene plasmid 10687). Retroviruses were produced by transfection of a *Patz1* cDNA in the pBabe-Puro (Addgene plasmid 1764) backbone with a plasmid encoding ecotropic retrovirus envelope proteins (pCL-Eco; Addgene plasmid 12371) in the HEK293T-Phoenix-Eco retroviral packaging cell line ([24], [25]). Viral supernatants were mixed with Polybrene (hexadimethrine bromide; 8 μg/ml) (catalog number H9268; Sigma-Aldrich), incubated with target cells for 3 h at 37°C, washed, and selected for 2 weeks in puromycin (1 μg/ml) (catalog number P9620; Sigma-Aldrich). Single colonies were identified, and PATZ1 overexpression was assessed by Western blotting. In all experiments, the DNA damage-inducing cytostatic drug doxorubicin (catalog number D1515; Sigma-Aldrich) was applied for the indicated times at a final concentration of 1 μM. Interacting proteins were treated *in vitro* with ethidium bromide (50 μg/ml) (catalog number E1510; Sigma-Aldrich) during immunoprecipitation.

Generation of shRNA-expressing cell lines. A *Patz1* short hairpin RNA (shRNA)-expressing pSM2 plasmid (RMM1766-96816118; GE

Healthcare-Open Biosystems) was modified and transferred into the pLMP retroviral expression plasmid (EAV4679; GE Healthcare-Open Biosystems), using EcoRI and XhoI restriction sites. Retrovirus production, infection, and selection were performed as stated above. Silencing of PATZ1 expression in NIH 3T3 cells was confirmed by Western blotting.

Luciferase assays. HCT116 p53$^{-/-}$, HEK293T, and HeLa cells were cotransfected with plasmids expressing p53, PATZ1, or PATZ1Alt with firefly luciferase reporter constructs that contained either the pG13 promoter (Addgene plasmid 16442), the mG15 promoter (Addgene plasmid 16443), the p21 gene promoter (Addgene plasmid 16451) ([26]), or the Puma gene promoter (Addgene plasmid 16591) ([27]), together with the renilla luciferase-encoding pRL-SV40 plasmid (Promega). Cells were harvested 48 h after transfection and analyzed with the Dual Luciferase reporter kit (catalog number E1960; Promega). Promoter activity was analyzed by normalizing firefly luciferase activity to renilla luciferase activity and adjusted to the fold increase over background.

Expression plasmids and oligonucleotides. The cytomegalovirus (CMV) promoter-driven FLAG-p53 expression plasmid was a kind gift from P. Ballar, Ege University, Izmir, Turkey. We sequenced this plasmid to ensure that the p53 cDNA that it carries is a WT allele. *Patz1*, *Patz1Alt*, and different *Patz1* truncations were cloned into pCMV-HA or pCMV-Myc (Clontech), using the EcoRI restriction enzyme site. *Patz1* and *Patz1Alt* cDNAs were also cloned into the pBABE-puro plasmid by using the EcoRI restriction enzyme site. p53α and p53β expression plasmids were a kind gift from J. C. Bourdon, University of Dundee. The sequences of oligonucleotides used in this study for amplification are available upon request.

Real-time cell growth and doubling time analysis. Cell proliferation was measured continuously with an xCELLigence real-time cell analyzer dual plate (RTCA DP) system (ACEA Biosciences, San Diego, CA), by seeding 5,000 cells into each well of an E-Plate View 16 tissue culture plate in 200 μl in 5% CO_2 at 37°C. Cell index (CI) measurements were taken every 15 min for up to 120 h. Doubling time analysis was restricted to the exponential growth phase.

Bacterial expression, *in vitro* binding, and EMSA. The PATZ1 cDNA was cloned into the bacterial expression plasmid pET28GST-LIC (Addgene plasmid 26101) by using isothermal assembly ([28]). Murine PATZ1 and human p53 (Addgene plasmid 24859) were expressed in the *Escherichia coli* host strain Rosetta2 DE3(pLys-S) ([29]). Protein expression was induced by the addition of 1 mM isopropyl-β-D-thiogalactopyranoside (IPTG) for 2 to 3 h. *E. coli* extracts were prepared by incubation in lysis buffer (25 mM Tris [pH 8.00], 500 mM NaCl, 1% Triton X-100, 10% glycerol), followed by centrifugation at 14 krpm. Glutathione *S*-transferase (GST) epitope-tagged PATZ1 was immobilized on glutathione-Sepharose beads (catalog number 17-5132-02; GE Healthcare), with or without p53, in immunoprecipitation (IP) buffer (25 mM Tris [pH 8.00], 100 mM KCl, 0.1% Triton X-100, 10% glycerol) overnight at 4°C and washed 8 times in ice-cold wash buffer (25 mM Tris [pH 8.00], 100 mM KCl, 2% Triton X-100). Protein contents of the bead conjugates were eluted in 1× Laemmli buffer. An electrophoretic mobility shift assay (EMSA) was performed with biotinylated p53 DNA probes (20 fmol) incubated with bacterial extracts containing p53 and/or PATZ1 (0.01 to 0.02 optical density at 550 nm [OD$_{550}$] unit equivalents) in EMSA binding buffer with 1 ng poly(dA-dT) (catalog number P0883; Sigma) for 1 h at 22°C and for 30 min at 4°C. Shifted bands were visualized by using streptavidin-coupled horseradish peroxidase (HRP), according to the manufacturer's instructions (Lightshift chemiluminescent EMSA kit, catalog number 20148; Thermo Scientific). The specificity of p53-dependent bands was demonstrated by competition with 40 or 80 pmol of unbiotinylated p53 probe or mutant p53 probe.

Cell lysis, immunoprecipitation, and DNA pulldown. Cells were lysed in hypotonic buffer (10 mM HEPES-KOH [pH 7.9], 2 mM $MgCl_2$, 0.1 mM EDTA, 10 mM KCl, 0.5% NP-40) and centrifuged at 14 krpm for 10 min, and supernatants were used for cytoplasmic extracts. Pellets were Dounce homogenized with 10 strokes in hypertonic buffer (50 mM

HEPES-KOH [pH 7.9], 2 mM $MgCl_2$, 0.1 mM EDTA, 50 mM KCl, 400 mM NaCl, 10% glycerol) for nuclear extraction. For immunoprecipitation, nuclear lysates (from 20×10^6 cells) were diluted at a 1:1 ratio in IP buffer (50 mM HEPES-KOH [pH 7.9], 5 mM $MgCl_2$, 100 mM KCl, 0.1% NP-40, 10% glycerol), incubated with anti-FLAG or antihemagglutinin (anti-HA) affinity gel or anti-p53 antibody-conjugated protein G-Sepharose beads at 4°C overnight, and washed 5 times in ice-cold wash buffer (50 mM HEPES-KOH [pH 7.9], 100 mM KCl, 2% NP-40).

For DNA pulldown, streptavidin-coupled Dynabeads (catalog number 11206D; Life Technologies, CA) were conjugated with biotinylated double-stranded p53 probes in $1\times$ bead-DNA binding buffer (5 mM HEPES-KOH [pH 7.9], 1 M NaCl, and 0.5 mM EDTA) at room temperature for 15 min and incubated with nuclear lysates from 3×10^6 cells in $1\times$ binding buffer [10 mM HEPES-KOH (pH 7.9), 50 mM NaCl, 0.5 mM EDTA, 1 mM $MgCl_2$, 20% glycerol, 0.01 μg/μl poly(dI/dC), 0.1 μg/μl bovine serum albumin (BSA), and 0.05% NP-40] at room temperature for 30 min. Protein contents of the bead conjugates were eluted in $1\times$ Laemmli buffer. Precipitated proteins were resolved on 10% SDS-PAGE gels and transferred onto polyvinylidene difluoride (PVDF) membranes (catalog number 88518; Thermo Fisher). Blots were incubated with peroxidase-coupled anti-HA, anti-FLAG, or anti-Myc antibodies; anti-PATZ1 antibody followed by protein A-peroxidase; or anti-p53 antibody followed by anti-mouse IgG–peroxidase. Reactivity was revealed by homemade enhanced chemiluminescence solutions made from Luminol (catalog number A4685; Sigma-Aldrich) and *p*-coumaric acid (catalog number C9008; Sigma-Aldrich) and visualized on SuperRX Fuji film. The intensities of bands in the Western blots were quantified with the ImageJ program (30).

Quantitative (real-time) reverse transcription-PCR (RT-PCR). Total mRNA was reverse transcribed by using a RevertAid first-strand cDNA synthesis kit with oligo(dT) primers (Fermentas). cDNA was amplified for 45 cycles (10 s at 95°C, 10 s at 52°C, and 10 s at 72°C) by using LightCycler 480 SYBR green I master mix (catalog number 04887352001; Roche) in a LightCycler 480 II instrument. Relative expression levels were calculated by using the $2^{-\Delta\Delta CP}$ method and normalized to the glyceraldehyde 3-phosphate dehydrogenase gene (*Gapdh*) expression level.

Site-directed mutagenesis. *Patz1* site-directed mutagenesis was performed by using a Phusion site-directed mutagenesis kit (catalog number F-541; Thermo Scientific), according to the manufacturer's instructions, using oligonucleotides abutting the target region. Briefly, a *Patz1* cDNA-containing plasmid was amplified, phosphorylated with polynucleotide kinase (catalog number M0201; NEB), ligated back onto itself, and transformed into bacteria. The R521Y/R527Y double mutant was generated by mutating the R521Y mutant by using R527 targeting oligonucleotides. The identities of the mutations were confirmed by bidirectional sequencing using primers EBV-rev and CMV-fwd.

Antibodies and reagents. The following antibodies were used in this study: anti-p53 clone 1C12 (catalog number 2524; Cell Signaling Technology), anti-PATZ1 H-300 (catalog number sc-292109; Santa Cruz Biotech), high-affinity anti-HA–peroxidase (catalog number 12013819001; Roche), monoclonal anti-FLAG M2 produced in mouse (catalog number F3165; Sigma), anti-c-Myc–peroxidase (catalog number 11814150001; Roche), anti-actin clone c4 (catalog number MAB1501; Merck-Millipore), anti-mouse IgG–peroxidase (catalog number A9044; Sigma), monoclonal anti-HA–agarose (catalog number A2095; Sigma), anti-FLAG M2 affinity gel (catalog number A2220; Sigma), Dynabeads protein A for immunoprecipitation (catalog number 1002D; Life Technologies), protein G-Sepharose beads (catalog number P3296; Sigma), and protein A-peroxidase (catalog number P8651; Sigma).

RNA-Seq analysis. Total mRNAs from early-passage *Patz1* WT or *Patz1⁻/⁻* MEFs were extracted by using TRIzol (catalog number 15596018; LifeTech) and poly(A) selected, and triplicate samples were sequenced at the Beijing Genomics Institute on an Illumina HiSeq 2000 sequencing machine. Raw fastq files were uploaded to GenePattern (version 3.8.1), and reads were mapped to the 2012 release of the *Mus muscu-*

lus genome (GRCm38.p2) by using the Bowtie aligner (Bowtie2 version 2.1.0) (31–33). The RNASeQC module (version 2) was used to perform quality control and to calculate metrics on aligned RNA-Seq data, including the calculated reads per kilobase of transcript per million mapped reads (RPKM) values for each transcript. Read counts were analyzed by using the R environment (R 3.0.2) and the DESeq package (version 1.18.0) according to suggestions reported previously (34). The DESeq algorithm estimates library size and variance and detects differentially expressed genes (DEGs) on the negative binomial distribution of the compared samples. DEGs with a fold change of >2 and a false discovery rate (FDR) value of < 0.01 were used for further analysis. To identify biological processes regulated by PATZ1, DAVID analysis was performed for gene ontology (GO) terms. *P* values were calculated with DAVID, and GO terms with *P* values of <0.01 were selected as being significant.

RNA-Seq data accession number. All RNA-Seq data are available in the GEO database (http://www.ncbi.nlm.nih.gov/geo/query/acc.cgi?acc=GSE65864) under accession number GSE65864.

RESULTS

Global effects of the absence of PATZ1 expression. To understand the function of PATZ1, we studied MEFs generated from *Patz1* gene-targeted C57BL/6 mice (16). We analyzed global gene expression in the presence or absence of *Patz1* gene products by RNA-Seq. We generated MEFs from *Patz1* wild-type (WT) or targeted (knockout [KO]) embryos at day 13.5 and isolated poly(A)-tailed RNA. These RNAs were sequenced by using the Illumina HiSeq 2000 platform and analyzed by using the R library DESeq. We identified 187 differentially expressed genes (DEGs), of which 97 were upregulated and 90 were downregulated in the absence of *Patz1* expression (data not shown). To identify biological processes dependent on *Patz1* expression, we performed DAVID analysis for gene ontology (GO) terms. We found unique biological processes that were associated with neuron differentiation; development; and, consistent with the previously identified functions of PATZ1, cell adhesion, morphogenesis, and proliferation (Fig. 1A). Notably, several genes known to be involved in cellular proliferation and also to be downstream of the p53 pathway were differentially regulated in the absence of PATZ1.

PATZ1 shortens cellular doubling time. Because genes related to cell proliferation were enriched among the differentially expressed genes in *Patz1*-deficient MEFs, we examined the growth rate of these cells. *Patz1⁻/⁻* MEFs proliferated significantly more slowly than did WT MEFs (Fig. 1B). Changes in the proliferation rate were evident by the calculated doubling time, which significantly increased for *Patz1⁻/⁻* MEFs (data not shown). This finding was consistent with the increased doubling times observed previously for MEFs generated from independent *Patz1⁻/⁻* mice (35). Conversely, PATZ1-overexpressing HCT116 human colon cancer cell lines proliferated faster and had decreased doubling times (Fig. 1C and data not shown). Furthermore, NIH 3T3 cells stably overexpressing *Patz1* cDNA displayed decreased doubling times, while cells expressing shRNA targeting all four products of the *Patz1* gene had longer doubling times (data not shown).

It is well known that the tumor suppressor p53 controls cellular proliferation. In our RNA-Seq analysis, among the genes enriched in GO terms related to cell proliferation, 8 genes were significantly affected by the absence of PATZ1. Among these genes are well-known p53 targets such as *Sfn* (14-3-3σ) and *Itgam* (6, 36) (Fig. 1A). Additionally, of the total 187 DEGs that we identified by comparing *Patz1* WT and KO MEFs, 24 genes were previously found to be basal p53 target genes (8). Moreover, 13 of these 187
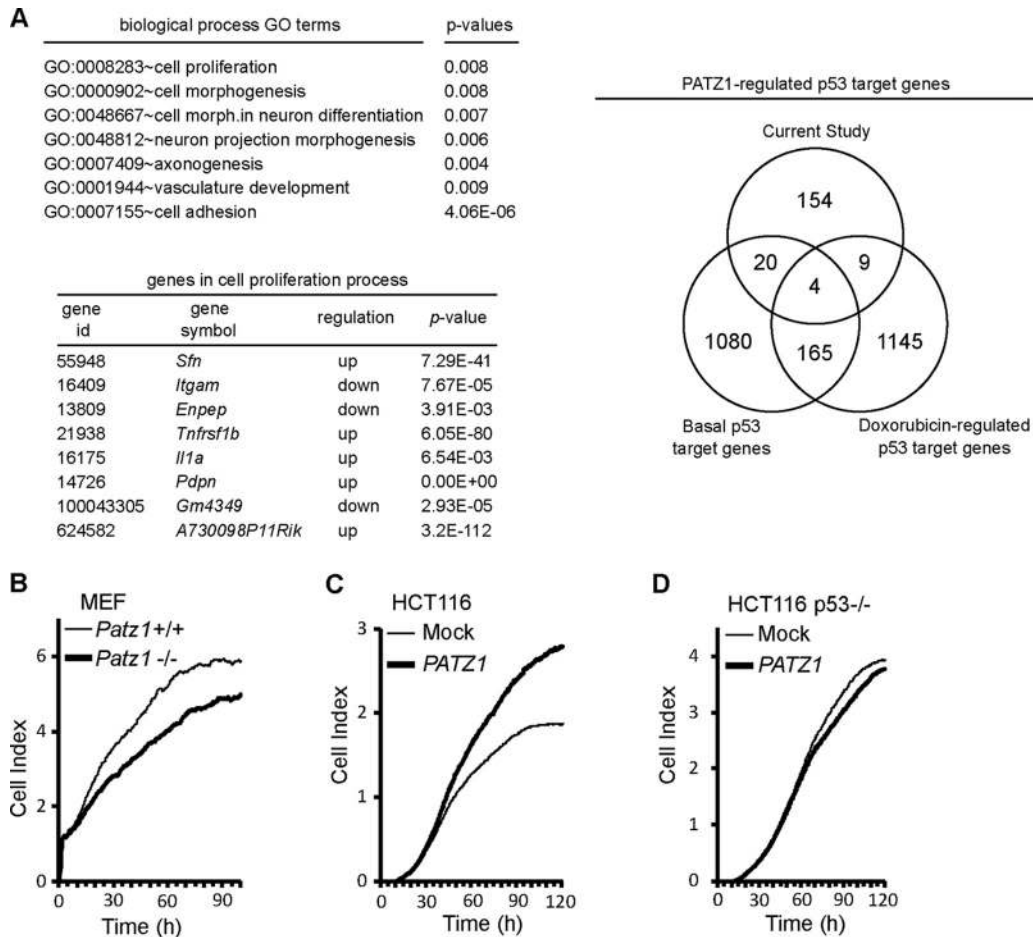
FIG 1 PATZ1 controls proliferation and inhibits cellular doubling time. (A) PATZ1-regulated biological processes in MEFs. Shown are biological process GO terms enriched in our WT versus *Patz1* KO DEG data set, with *P* values calculated by DAVID (45). Eight DEGs involved in cell proliferation are listed. The overlap of 187 PATZ1-regulated DEGs with well-characterized basal (1,269) and doxorubicin-regulated (1,323) p53 target genes reported previously by Kenzelmann Broz et al. is shown as a Venn diagram on the right (8). (B) PATZ1 expression is positively correlated with cell growth rate. (C) PATZ1 overexpression accelerates the growth of HCT116 cells. (D) PATZ1 cannot increase the growth rate of HCT116 cells in the absence of p53. Growth curves of *Patz1*$^{-/-}$ and wild-type MEFs (B), HCT116 cells (C), and HCT116 p53$^{-/-}$ cells (D) were visualized on an xCELLigence RTCA DP system.

PATZ1 DEGs were identified to be doxorubicin-regulated p53 targets (data not shown). Therefore, we examined the p53 dependence of the role of PATZ1 in cellular proliferation. To this end, we analyzed the growth of p53$^{-/-}$ HCT116 cells overexpressing PATZ1. We found that PATZ1 was unable to enhance cellular proliferation in p53-deficient HCT116 cells (Fig. 1D). Thus, in various cellular systems, PATZ1 activates cellular proliferation in a p53-dependent manner.

PATZ1 is downregulated upon DNA damage. The mouse and human *Patz1* genes express 4 major alternatively spliced transcripts: mPATZ1-004, -001, -012, and -003 (corresponding to hPATZ1-001, -004, -002, and -003, respectively), which encode 74-, 69-, 58-, and 57-kDa proteins, respectively. We analyzed the expression of these isoforms by exon-specific amplification and found that all four isoforms were expressed in various mouse and human cell lines (data not shown). In this study, we annotated the most commonly investigated 69-kDa mPATZ1-001 (hPATZ1-004) and 58-kDa mPATZ1-012 (hPATZ1-002) isoforms PATZ1 and PATZ1Alt, respectively, for simplicity.

To further investigate the role of PATZ1 in p53-dependent

gene expression, we treated MEFs with the DNA damage-inducing cytostatic drug DOX and studied the well-established p53 response. As expected, p53 levels of untreated MEFs were low and rapidly induced upon treatment with DOX (Fig. 2A, bottom). In stark contrast, PATZ1 proteins were significantly lost after 16 h of treatment and did not recover upon further treatment (Fig. 2A, top). We further treated HCT116 cells with DOX and found that PATZ1 was again lost after 24 h of treatment (Fig. 2B, top). Because PATZ1 loss correlated with p53 induction after DOX treatment, we questioned whether p53 was necessary for this phenomenon (Fig. 2B, middle). We treated HCT116 p53$^{-/-}$ cells with DOX and found that PATZ1 loss was still evident even in the absence of p53 (Fig. 2B, top). To determine if PATZ1 loss was mediated by alterations in the steady-state levels of *Patz1* mRNA, we measured mRNA levels by quantitative real-time PCR but could not detect significant changes in the time range where PATZ1 protein levels dramatically decrease (Fig. 2C). Thus, DOX treatment results in the loss of PATZ1, while p53 levels dramatically increase.

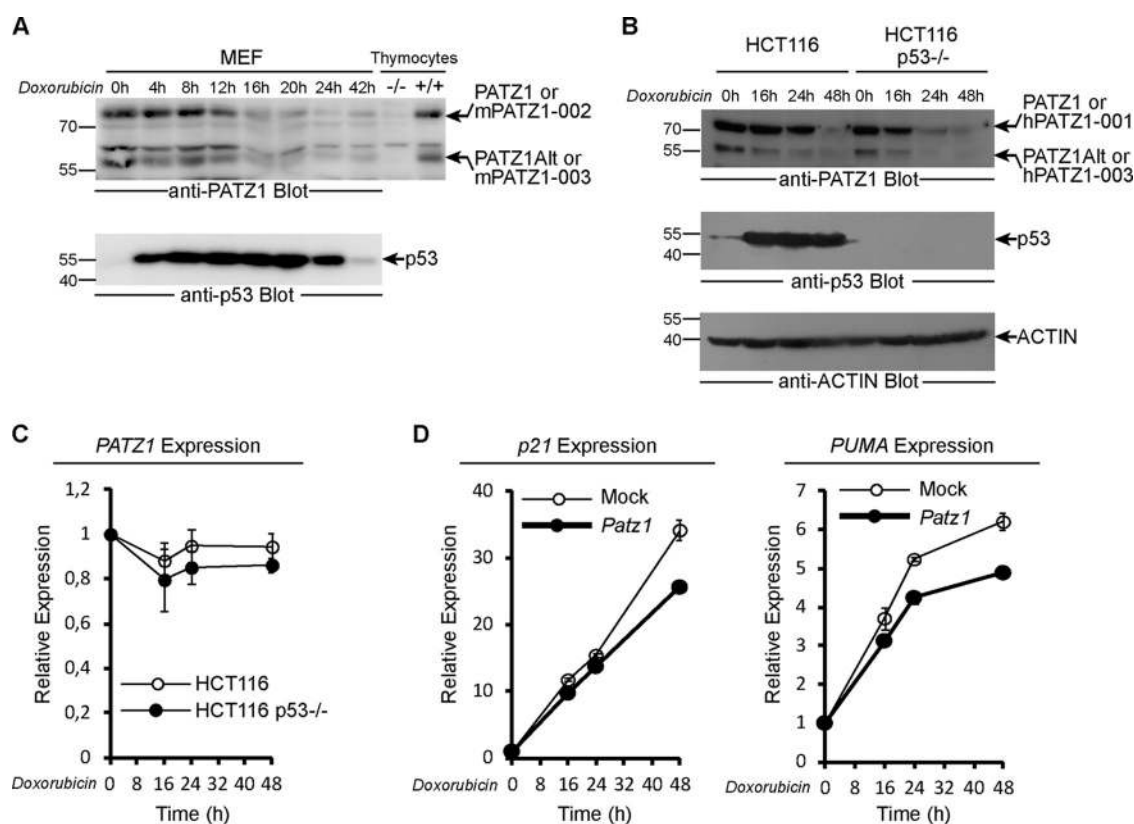To reveal the significance of PATZ1 loss for p53 activity, we

FIG 2 PATZ1 is downregulated upon DNA damage. (A) Downregulation of PATZ1 in DOX-treated MEFs. Whole-cell lysates from MEFs treated with 1 μM DOX for the indicated times were immunoblotted with anti-PATZ1 (top) and anti-p53 (bottom) antibodies. The presence of PATZ1 isoforms and p53 is indicated by arrows. (B) Downregulation of PATZ1 alternative splice variants in HCT116 (p53 WT or p53$^{-/-}$) cells treated with 1 μM DOX for the indicated times. (Top and middle) Whole-cell lysates were immunoblotted with anti-PATZ1 (top) and anti-p53 (middle) antibodies. (Bottom) Equal loading was confirmed by blotting of the same membrane with antiactin antibodies, revealing equal amounts of a 40-kDa actin band. (C) DOX treatment does not alter mRNA levels of *PATZ1*. *PATZ1* mRNAs from HCT116 p53 WT or HCT116 p53$^{-/-}$ cells treated with 1 μM DOX for the indicated times were quantified by real-time PCR. *PATZ1* expression was normalized to *Gapdh* expression. (D) Loss of PATZ1 activates p53 function. Quantitative RT-PCR analysis reveals higher p53-dependent gene transcript levels at time points where PATZ1 is lost upon DNA damage. Mock-infected cells express more p21 (left) and Puma (right) than do PATZ1-overexpressing cells after 48 h of DOX treatment.

examined the expression of the endogenous *p21* and *PUMA* genes, which are known to be induced by DNA damage in a p53-dependent way. As expected, *p21* and *PUMA* gene expression levels increased upon DOX treatment in HCT116 cells. Significantly, PATZ1 overexpression blunted this p53-dependent increase, especially at later time points where endogenous PATZ1 was lost (Fig. 2D). We conclude that PATZ1 can inhibit p53-dependent transcription activation.

PATZ1 interacts with p53. To identify the mechanism of the role of PATZ1 in p53 inhibition, we assessed the direct association of these two transcription factors. We expressed epitope-tagged versions of these proteins in *E. coli* and demonstrated that PATZ1 and p53 interact *in vitro* in GST pulldown experiments (Fig. 3A). We examined the subcellular localization of the long (74- and 69-kDa) and short (58- and 57-kDa) PATZ1 isoforms and found that unlike p53, which shuttles between the cytoplasm and the nucleus, PATZ1 isoforms remain predominantly nuclear. Nuclear localization was independent of both DOX treatment and the presence of p53 (data not shown). To assess whether endogenous PATZ1 and p53 physically interact, we examined the association between these two proteins in HCT116 cells with or without p53 expression, in the presence or absence of DOX treatment. As ex-

pected, DOX dramatically increased the levels of cellular p53 (Fig. 3B, middle). Anti-p53 immunoprecipitates immunoblotted with an antibody against the N-terminal BTB domain revealed that the long and short PATZ1 isoforms interact with p53. Importantly, upon short-term DOX treatment (8 h), before PATZ1 degradation was evident (Fig. 3B, bottom), the amount of PATZ1 bound to p53 did not change (Fig. 3B, top).

PATZ1 can bind to p53 as a heterodimer. To study this interaction in more detail, we overexpressed HA epitope-tagged PATZ1 or PATZ1Alt along with FLAG epitope-tagged p53 in HCT116 p53$^{-/-}$ cells. We found that only PATZ1 and not the PATZ1Alt variant could bind p53 (Fig. 3C), an unexpected result given our above-described observation that p53 antibodies could immunoprecipitate both long and short endogenous isoforms. The inconsistency between the interaction specificities of the endogenous and overexpressed proteins could be explained in two ways. The endogenous short PATZ1 isoform could consist of the hPATZ1-003 and/or PATZ1Alt variant. One possibility is that only hPATZ1-003 but not PATZ1Alt interacts with p53. Alternatively, the endogenous hPATZ1-003 and PATZ1Alt variants could be indirectly interacting with p53 in multiprotein complexes. To address these possibilities, we tested whether PATZ1Alt het-
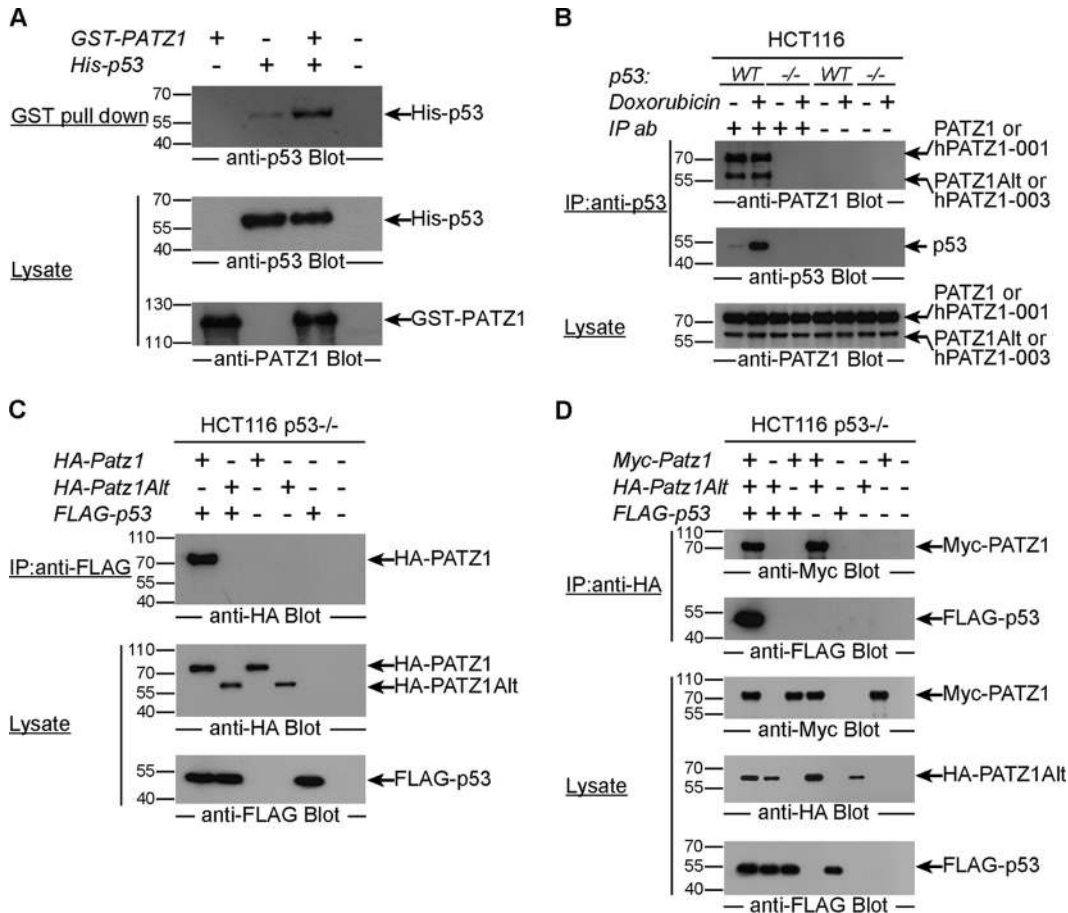
FIG 3 PATZ1 binds p53. (A) Interaction of bacterially expressed PATZ1 and p53. (Top) Glutathione bead capture of GST epitope-tagged PATZ1 followed by anti-p53 Western blotting reveals PATZ1-bound p53 (lane 3). (Middle and bottom) Bacterial lysates show that GST-PATZ1 (middle) and His-p53 (bottom) are present at equal levels. (B) Endogenous PATZ1 interacts with p53 in HCT116 cells. (Top) Anti-p53 immunoprecipitation followed by anti-PATZ1 antibody (ab) blotting reveals the presence of long and short isoforms of PATZ1 in complex with p53 in HCT116 cells in the absence (lane 1) or presence (lane 2) of DOX treatment. Binding is specific, as immunoprecipitates from HCT116 p53$^{-/-}$ cells (lanes 3 and 4) do not reveal the presence of PATZ1 or PATZ1Alt. (Middle) Anti-p53 immunoprecipitation followed by anti-p53 antibody blotting reveals that DOX treatment induces p53 expression (lanes 1 and 2). (Bottom) Lysates show that long and short isoforms of the PATZ1 protein are expressed at equal levels. (C) Overexpressed PATZ1 interacts with overexpressed p53. (Top) Anti-FLAG immunoprecipitation followed by anti-HA antibody blotting reveals the presence of HA-PATZ1 but not HA-PATZ1Alt in HCT116 p53$^{-/-}$ cells transfected with the indicated plasmids. (Middle and bottom) Lysates of transfected cells show that HA-PATZ1 and HA-PATZ1Alt (middle) as well as FLAG-p53 (bottom) are expressed at equal levels in transfected cells. (D) PATZ1Alt can interact with p53 only in the presence of PATZ1. (Top) Anti-HA immunoprecipitation followed by anti-Myc antibody blotting reveals the presence of a complex of Myc-PATZ1 and HA-PATZ1Alt (lanes 1 and 3). (Second panel) Anti-HA immunoprecipitation followed by anti-FLAG antibody blotting reveals the presence of an HA-PATZ1Alt–FLAG-p53 complex only in the presence of Myc-PATZ1 (lane 1). (Bottom panels) Lysates of transfected HCT116 p53$^{-/-}$ cells blotted with anti-Myc, anti-HA, and anti-FLAG show that PATZ1, PATZ1Alt, and p53 proteins are expressed at equal levels.

erodimerizes with PATZ1 and indirectly coimmunoprecipitates with p53. We overexpressed Myc-PATZ1 and HA-PATZ1Alt along with FLAG-p53 in HCT116 p53$^{-/-}$ cells. We found that PATZ1 and PATZ1Alt could indeed heterodimerize (Fig. 3D, top). Moreover, PATZ1Alt associated with p53 only in the presence of PATZ1 (Fig. 3D, second panel).

The N-terminal BTB domain is required for PATZ1-PATZ1Alt heterodimerization. Previous studies demonstrated that BTB domains mediate homo- or heterodimerization (37). In fact, PATZ1 could form homodimers by using its N-terminal BTB domain (19). To identify the domain that is required for the PATZ1-PATZ1Alt heterodimer, we generated various expression constructs encoding PATZ1 truncation mutants. These truncations contained (i) PATZ1 lacking its ZF domain (Myc-ΔZF), (ii) PATZ1 with only the BTB domain (Myc-BTB), or (iii) PATZ1

lacking its BTB domain (Myc-ΔBTB) (Fig. 4A). We cotransfected HCT116 cells with HA-PATZ1Alt with either full-length Myc-PATZ1 or its truncated variants. All of these expression constructs resulted in the expression of equivalent levels of truncated proteins (Fig. 4B, bottom). The BTB domain was indeed necessary for the PATZ1-PATZ1Alt interaction, as all truncated PATZ1 variants except the truncation lacking the BTB domain bound PATZ1Alt. In fact, the BTB domain by itself was sufficient to heterodimerize with the PATZ1Alt protein (Fig. 4B, top). Thus, PATZ1 can not only homodimerize but also heterodimerize with PATZ1Alt. Moreover, these PATZ1-PATZ1Alt heterodimers retain the ability to associate with p53.

p53 binds to the C terminus of PATZ1. As p53 binds only PATZ1 and not PATZ1Alt, we assessed the domain requirements of the p53-PATZ1 interaction in more detail. Because the PATZ1
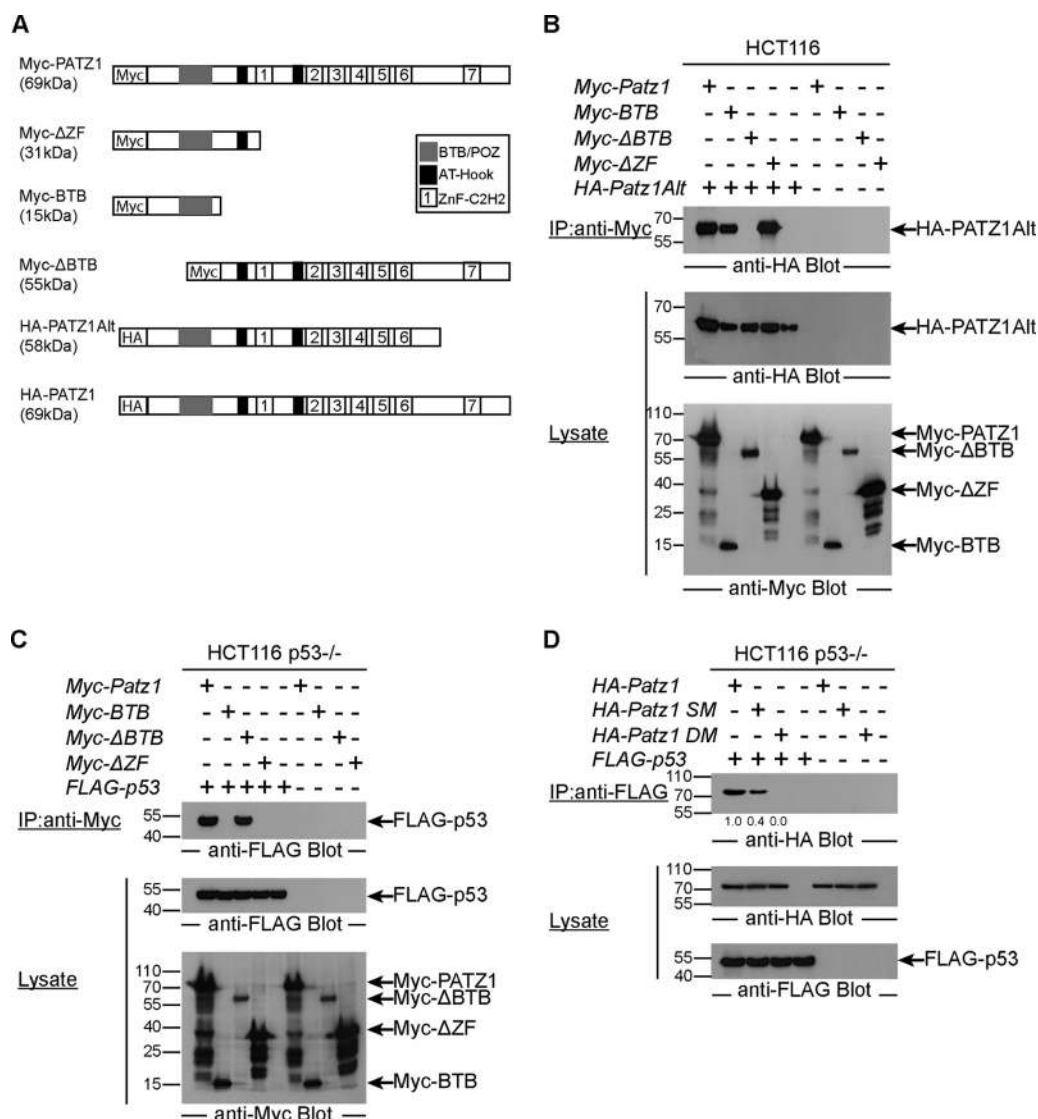
FIG 4 The C-terminal tail of PATZ1 is required for binding p53. (A) Schematic representation of PATZ1 truncations. N-terminal epitope tags are indicated by boxes with HA or Myc. The names and expected molecular masses of the PATZ1 truncations are indicated on the left. (B) BTB domains are necessary for PATZ1 and PATZ1Alt heterodimerization. (Top) Anti-Myc immunoprecipitation followed by anti-HA antibody blotting reveals the presence of a complex of Myc-PATZ1 and HA-PATZ1Alt only in cells expressing BTB containing Myc-PATZ1 proteins (lanes 1, 2, and 4). Myc-ΔBTB cannot bind to HA-PATZ1Alt (lane 3). (Middle and bottom) Lysates of transfected HCT116 cells blotted with anti-HA and anti-Myc show that PATZ1, truncation variants of PATZ1, and PATZ1Alt proteins are expressed at equal levels. (C) The C-terminal ZFs of PATZ1 are necessary for p53 binding. (Top) Anti-Myc immunoprecipitation followed by anti-FLAG antibody blotting reveals the presence of FLAG-p53 in complex with Myc-PATZ1 (lane 1) and Myc-ΔBTB (lane 3) but not Myc-BTB (lane 2) or Myc-ΔZF (lane 4) in HCT116 p53$^{-/-}$ cells transfected with the indicated plasmids. Binding is specific, as no coimmunoprecipitation is evident in lysates lacking FLAG-p53 (lanes 6 to 9). (Middle and bottom) Lysates of transfected cells show that FLAG-p53 (middle) and Myc-PATZ1 and its truncations (bottom) are expressed at equal levels in transfected cells. Some Myc epitope-tagged PATZ1 truncations revealed lower-molecular-weight degradation products, but the proteins of interest at the expected size are indicated by arrows on the right. (D) Negatively charged residues in the ZF domain are required for PATZ1-p53 binding. (Top) Anti-FLAG immunoprecipitation followed by anti-HA antibody blotting reveals the presence of HA-PATZ1 (lane 1) in complex with FLAG-p53 in HCT116 p53$^{-/-}$ cells transfected with the indicated plasmids (top). PATZ1 with a single mutation (HA-PATZ1 SM) has attenuated binding to p53 (lane 2), while PATZ1 with a double amino acid mutation (HA-PATZ1 DM) cannot bind p53 (lane 3). Binding is specific, as no coimmunoprecipitation is evident in lysates lacking FLAG-p53 (lanes 5 to 8). (Middle and bottom) Lysates of transfected cells show that HA-PATZ1 and its mutants (middle) and FLAG-p53 (bottom) are expressed at equal levels in transfected cells.

and PATZ1Alt proteins are identical in their N termini and differ only after the sixth ZF motif in their DNA binding domains, we speculated that it was the C-terminal region of PATZ1 that mediated the interaction with p53. Indeed, only the PATZ1 truncations that contained the C-terminal ZF domain could interact with p53 (Fig. 4C, top). We also conclude that homodimerization of

PATZ1 is not required for the p53-PATZ1 interaction, as PATZ1 lacking its BTB dimerization domain continued to bind p53 (Fig. 4C, top).

To characterize the PATZ1-p53 interaction surface, we analyzed the amino acid sequence of the C-terminal region of PATZ1, which is necessary for p53 binding. The region of PATZ1 between

ZF6 and ZF7 is highly conserved and negatively charged (data not shown). We hypothesized that if these negatively charged amino acids were forming an interaction surface necessary to bind p53, large, noncharged amino acid substitutions would disrupt this interaction. To this end, we generated single (D521Y) and double (D521Y/D527Y) site-directed mutant versions of the HA-*Patz1* cDNA. HCT116 p53$^{-/-}$ cells transfected with either WT or mutant HA-*Patz1* constructs expressed equivalent levels of PATZ1 (Fig. 4D, middle). We found that residues 521 and 527 of PATZ1 were necessary for the p53 interaction because the single and double mutants, respectively, bound p53 at only reduced (40%) or undetectable levels (Fig. 4D).

Ethidium bromide is a known DNA intercalator that disrupts protein-DNA interactions (38). Even though PATZ1 and p53 interact in nuclear lysates, this interaction was not affected by ethidium bromide and therefore did not require the presence of DNA (data not shown). The PATZ1-p53 interaction was also stable in cells undergoing DNA damage (data not shown). Thus, the interaction between PATZ1 and p53 in the nucleus requires a negatively charged region between ZF motifs 6 and 7 in the C-terminal domain, and an alternative splice variant, PATZ1Alt, cannot directly bind p53.

PATZ1 inhibits p53 function. To study the functional significance of the PATZ1-p53 interaction, we performed luciferase reporter assays. We first tested whether PATZ1 could affect the ability of p53 to activate transcription from the well-established pG13 reporter, which contains 13 copies of a consensus p53 binding site driving luciferase gene expression. As expected, p53 specifically activated transcription from this construct when cotransfected into HCT116 p53$^{-/-}$ cells (Fig. 5, top). PATZ1 or PATZ1Alt expression by itself did not activate transcription from this construct, while PATZ1 and p53 coexpression resulted in a 3-fold decrease in p53 activity. We also observed dramatic decreases in p53-dependent transcription activation in HeLa and HEK293T cells when PATZ1 was overexpressed (data not shown). In these experiments, PATZ1Alt did not decrease p53 activity as effectively as did PATZ1, consistent with its inability to interact with p53. Furthermore, PATZ1Alt did not have a dominant negative effect on PATZ1, as it did not interfere with the function of PATZ1 on p53. We found that PATZ1 could also inhibit the ability of p53 to activate transcription from the *CDKN1A* (*p21*) or *BBC3* (*PUMA*) gene promoters (Fig. 5, middle and bottom).

Next, we assessed the domain requirements of p53 for the interaction with and inhibition by PATZ1. To this end, we used wild type (p53α) or a naturally occurring alternative splice version (p53β) missing the C-terminal regulatory domain (39). As expected, PATZ1 coexpression dramatically inhibited p53α-dependent transcription. In contrast, PATZ1 could not directly bind or effectively inhibit p53β (data not shown). Thus, the interaction between PATZ1 and p53 requires the C-terminal domains of both proteins.

PATZ1 inhibits p53 DNA binding. To understand the mechanism of p53 inhibition by PATZ1, we assessed p53 DNA binding in the presence or absence of PATZ1. We performed electrophoretic mobility shift assays (EMSAs) with biotinylated p53 probes (derived from the pG13 reporter) incubated with bacterial extracts containing p53 and/or PATZ1. Incubation of p53 with DNA probes resulted in a specific shifted band, the intensity of which dramatically decreased when p53 was present together with PATZ1 (Fig. 6A). Thus, PATZ1 directly inhibits p53 DNA bind-
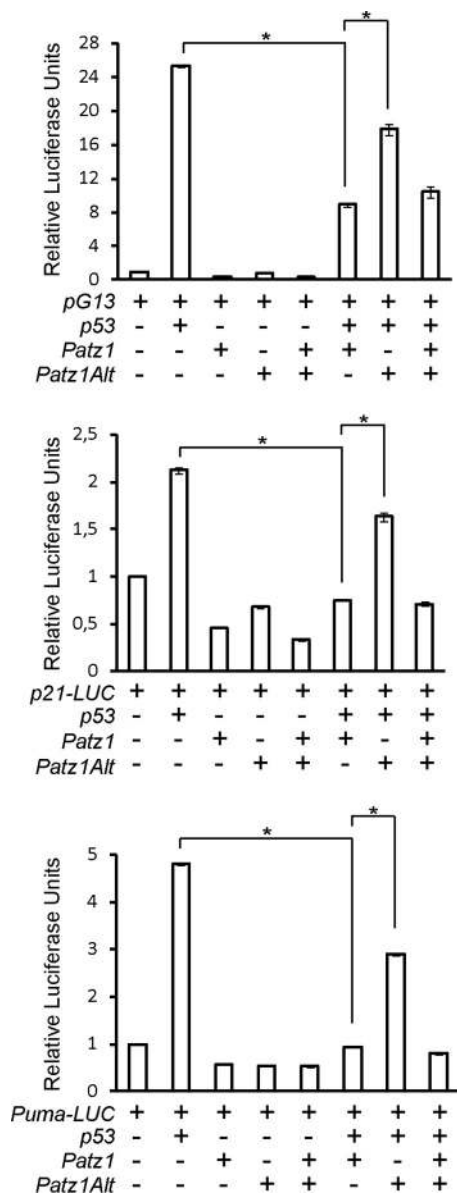

FIG 5 PATZ1 inhibits p53 function. PATZ1 inhibits p53 activity in luciferase assays. (Top) HCT116 p53$^{-/-}$ cells transfected with different combinations of the pG13 p53-dependent luciferase vector and FLAG-p53, PATZ1, and PATZ1Alt expression plasmids. p53 specifically activates the pG13 reporter (columns 1 and 2), while PATZ1 and PATZ1Alt cannot (columns 3 and 4). PATZ1 but not PATZ1Alt can inhibit p53 activity (columns 5 and 6). (Middle and bottom) The same experiment was conducted with the p21 promoter luciferase construct (middle) and the Puma promoter luciferase construct (bottom).

ing. To study the inhibition of p53 DNA binding by PATZ1 in detail, we overexpressed FLAG-p53 and HA-PATZ1 or PATZ1Alt variants in HCT116 p53$^{-/-}$ cells and performed pulldown experiments with biotinylated double-stranded DNA probes that were captured with streptavidin-conjugated magnetic beads. We found that PATZ1, which can directly bind to p53, inhibited p53 DNA binding 5-fold. On the other hand, PATZ1Alt, which does not bind p53, did not inhibit p53 DNA binding. Neither PATZ1 nor PATZ1Alt could bind directly to this p53 binding-site DNA probe

(p53 probe 1; identical to the EMSA probe) (Fig. 6B). PATZ1 could prevent p53 DNA binding even in the presence of PATZ1Alt. To understand the importance of the PATZ1-p53 interaction in the inhibition of p53 DNA binding, we assessed the ability of PATZ1 site-directed mutants that cannot bind to p53 to inhibit p53 DNA binding. Like PATZ1Alt, single and double point mutants of PATZ1 could not effectively prevent p53 DNA binding (Fig. 6C, left). Quantification of DNA-bound p53 demonstrated that the ability of PATZ1 to bind p53 was directly proportional to its affinity for p53 (Fig. 6C, right). We conclude that PATZ1 can directly interact with p53 to prevent it from binding its consensus DNA site.

To generalize the finding that PATZ1 inhibits p53 DNA binding, we repeated this pulldown experiment with a different DNA probe that contained p53 binding sequences from the *Gadd45* gene promoter (probe 2). Again, we observed that PATZ1 inhibited p53 DNA binding (Fig. 6D). Unexpectedly, PATZ1 also bound this DNA probe, competed with p53, and contributed to the inhibition of p53 DNA binding (Fig. 6D, second panel). Thus, PATZ1 can inhibit p53 DNA binding by two mechanisms: first by forming a complex with p53 and preventing p53 DNA binding and second by competing for some p53 binding sites and displacing DNA-bound p53.

We next tested whether p53 could also inhibit PATZ1 from binding to its specific DNA probe (from the *Cd8* gene locus). In fact, in the presence of p53, 50% less PATZ1 bound this probe (Fig. 6E, top). Surprisingly, PATZ1Alt bound this probe more efficiently than did PATZ1, yet p53, which is incapable of binding PATZ1Alt, could not inhibit PATZ1Alt DNA binding (Fig. 6E, right). Thus, PATZ1 and p53 interact to form a complex that is incapable of binding the target sites of the individual proteins.

DISCUSSION

This study identifies the mechanism of interaction between the inhibitory transcription factor PATZ1 and the p53 tumor suppressor protein. RNA-Seq analysis demonstrates that the deficiency of PATZ1 affects various biological processes, one of which is cellular proliferation. We confirmed that PATZ1 is an activator of proliferation with real-time measurements. Moreover, this role of PATZ1 is p53 dependent, as the proliferative capacity of p53-deficient cells is not affected by the overexpression of PATZ1. Significantly, we find that the 69-kDa PATZ1 variant can bind p53 but that the 58-kDa PATZ1Alt variant cannot. This interaction does not require other cellular complexes, as recombinant PATZ1 and p53 continue to interact *in vitro*. PATZ1 binds p53 by using a negatively charged region buried between the sixth and seventh ZF motifs in the DNA binding domain. In fact, we find that two aspartic acid residues (D521 and D527) are necessary for this interaction. The interaction of PATZ1 with p53 inhibits p53 DNA binding and p53-dependent transcription activation.

Our RNA-Seq experiments comparing the *Patz1* deficiencies of DEGs reveal critical roles for this transcription factor in cell adhesion, neuron development, morphogenesis, and cellular proliferation. The association of PATZ1 deficiency with these processes sheds light on recent findings showing that *Patz1*$^{-/-}$ mice are born with defects in their central nervous system (35). Moreover, the finding that *Patz1*$^{-/-}$ mice are small could be explained by the list of DEGs related to proliferation in our RNA-Seq experiments (16, 17). Consistently, our findings on the alteration of the cellular

doubling time in the presence or absence of PATZ1 support the function of this protein in cellular proliferation. Significantly, the identification of 33 known p53 target genes as DEGs in PATZ1 deficiency links these two transcription factors.

In this study, we find that PATZ1 proteins are sensitive to DNA damage. At early time points after DNA damage, p53 is rapidly induced, while PATZ1 levels remain constant, where these two proteins coexist and interact. Thus, the decrease of PATZ1 levels is likely a result of and not causal to p53 induction. At later time points after DNA damage, the protein levels of p53 and PATZ1 are inversely correlated. We observed that in contrast to p53-deficient cells, those with wild-type p53 had delayed PATZ1 degradation, especially after long exposure to genotoxic DOX. The decreases in PATZ1 levels are not regulated by the interaction of PATZ1 with p53, as PATZ1Alt, which does not bind to p53, is degraded with kinetics similar to those of PATZ1. As PATZ1 promotes proliferation, its downregulation after DNA damage may point to its role in p53-dependent cell cycle control. Consistent with this idea, we observed that upon long-term DOX treatment, as PATZ1 protein levels decrease, p53 target gene expression levels increase. Moreover, overexpression of PATZ1 in this setting reduces this effect. The mechanism of DNA damage-dependent PATZ1 loss is likely due to ubiquitination-dependent proteasomal degradation and is currently being investigated.

PATZ1 has an N-terminal BTB domain and a C-terminal DNA binding domain composed of ZF motifs. The BTB/POZ domain mediates homo- and heterodimerization as well as protein-protein interactions resulting in the recruitment of corepressor complexes. PATZ1 uses its BTB domain to heterodimerize with other BTB proteins such as BCL-6 and Bach (19, 40, 41). Here we also find that the alternatively spliced variants of PATZ1 use their BTB domains to heterodimerize with each other. An open question is the stoichiometry of the p53-PATZ1 complex. While PATZ1 can clearly homo- and heterodimerize, it is not known if PATZ1, like p53, can tetramerize. We demonstrate here that truncated PATZ1 proteins without a BTB domain, which cannot homo- or heterodimerize, can still bind p53 (Fig. 4C).

The inability of the p53β alternative splice variant to bind PATZ1 indicates that PATZ1 associates with the C-terminal regulatory domain of p53. A previous *in vitro* binding study also confirms that PATZ1 binds to the C-terminal domain of p53 (17). The region surrounding amino acid K382 of p53 is homologous to that of histone H4K20 (42). In fact, our preliminary experiments indicate that PATZ1 could also bind to H4K20. This is precisely the region that 53BP1 recognizes in both p53 and histone H4, suggesting that PATZ1 can potentially compete with 53BP1 for p53 binding (43, 44). 53BP1 uses its Tudor domain to bind p53; however, PATZ1 does not present any homology to Tudor domains.

We find that PATZ1 can bind p53, independent of DOX-induced DNA damage. Induction of DNA damage stabilizes and dramatically increases the amount of nuclear p53; however, the amount of PATZ1 that binds to p53 before and after DNA damage remains constant. Thus, it is possible that limiting PATZ1 levels determine the amount of PATZ1-p53 complexes. If this is the case, we would expect to find an abundant pool of PATZ1-unbound p53 in stressed cells.

Of the two p53 REs that we used in this study, probe 1 contains only one decamer half-site, while probe 2 has two adjacent decamer half-sites (from the pG13 artificial reporter
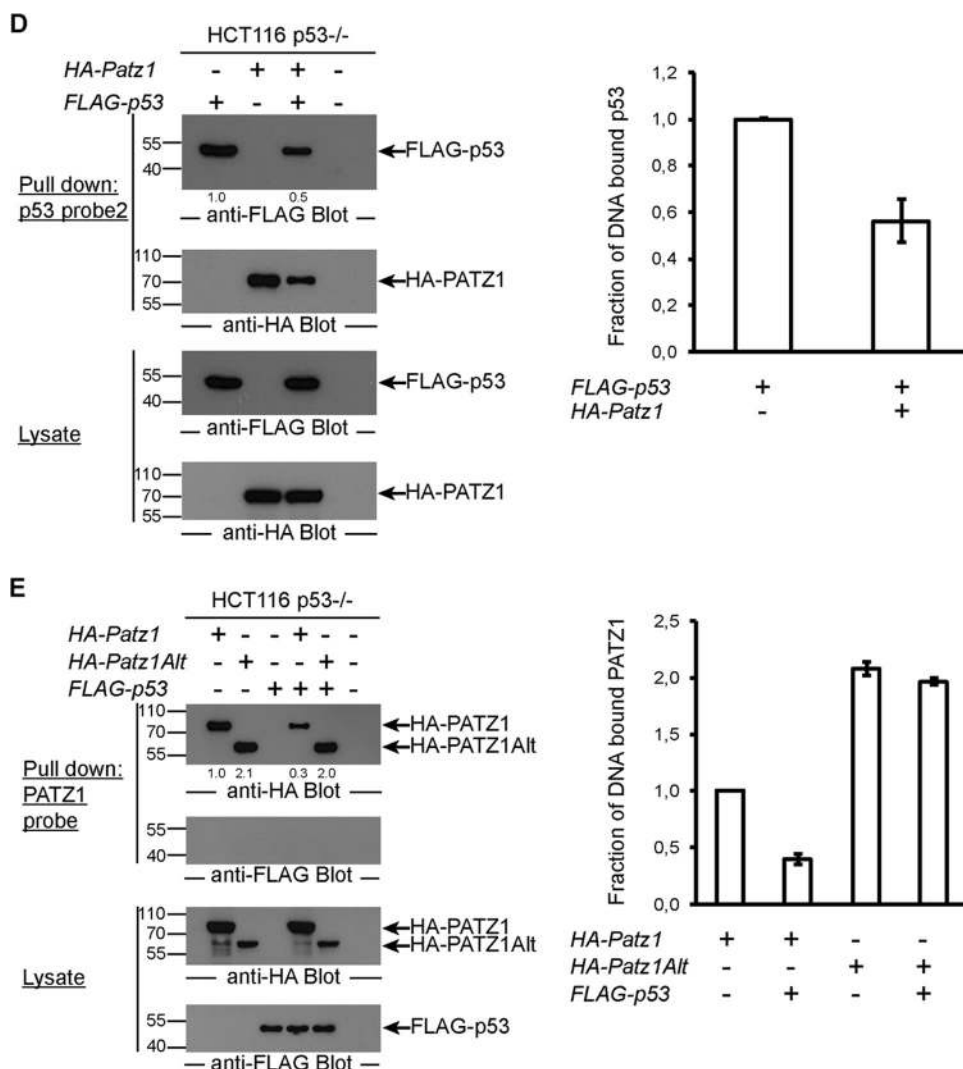
and the *Gadd45* gene promoter, respectively). Binding of p53 to both of these probes is inhibited by its association with PATZ1, as shown by EMSA and DNA pulldown experiments. Our site-directed mutagenesis experiments reveal that the amount of probe-bound p53 is inversely correlated with the affinity of PATZ1 for p53. Conversely, p53 inhibits the binding of PATZ1 to probes containing its REs. Surprisingly, we find that PATZ1 can also bind p53 probe 2, effectively excluding p53 from its target site. Thus, PATZ1 can inhibit p53 DNA binding in two ways. First, PATZ1-bound p53 cannot bind its consensus DNA binding sites; second, PATZ1 can compete for DNA probes containing some p53 sites.

p53 binds its REs as tetramers (Fig. 7A and B). Here we demonstrate that PATZ1 homodimers or PATZ1-PATZ1Alt heterodimers form complexes with p53 and remove it from DNA (Fig. 7C). In return, p53 can also remove PATZ1 from its binding sites. These findings indicate that PATZ1 and p53 form a complex that is incapable of binding DNA. The selective deregulation of p53 target genes in PATZ1-deficient cells observed by RNA-Seq correlates with the inhibitory effect of PATZ1 on p53 DNA binding in pulldown experiments. This study definitively reports that the BTB-ZF transcription factor PATZ1 can interact with and inhibit the DNA binding and transcriptional activity of p53.

FIG 6 PATZ1 inhibits p53 DNA binding. (A) p53 DNA binding in EMSAs is inhibited by PATZ1. Incubation of bacterially expressed His-tagged p53 with biotinylated p53 probes reveals a specific shifted band (lane 2). The specificity of this band was demonstrated by competition using an unlabeled p53 probe (lanes 3 and 4) and an unlabeled mutant p53 probe (lanes 5 and 6). Decreased levels of p53-dependent shifted bands are evident in the presence of PATZ1 (lanes 7 and 8). Triangles represent 2-fold increasing amounts of PATZ1 and competitor probes. *ns indicates a nonspecific band that cannot be competed away with competitor probes. (B) The PATZ1-p53 interaction inhibits p53 DNA binding to probe 1, derived from the pG13 p53 reporter. (Top and second panels) Precipitation followed by anti-FLAG (top) or anti-HA (second panel) antibody blotting reveals the presence of DNA-bound FLAG-p53 but not HA-PATZ1 (top, lane 1). FLAG-p53 continues to bind to DNA in the presence of HA-PATZ1Alt (top, lane 5) but not HA-PATZ1 (lane 4). (Third and bottom panels) Lysates of transfected cells show that FLAG-p53 (third panel) and HA-PATZ1 and HA-PATZ1Alt (bottom) are expressed at equal levels in transfected cells. The intensities of the relevant bands were quantified and normalized to the intensity of the lane with FLAG-p53 alone (indicated as values below the top panel). (C) PATZ1 mutants that do not bind p53 cannot inhibit p53 DNA binding. (Top and second panels) Precipitation followed by anti-FLAG (top) or anti-HA (second panel) antibody blotting reveals the presence of DNA-bound FLAG-p53 (lane 1). FLAG-p53 continues to bind to DNA in the presence of HA-PATZ1 DM (lane 7). Less FLAG-p53 is bound to DNA in the presence of HA-PATZ1 SM (lane 6), and dramatically reduced binding is seen in the presence of HA-PATZ1 (lane 5). (Third and bottom panels) Lysates of transfected cells show that FLAG-p53 (third panel) and HA-PATZ1 and the single and double mutants HA-PATZ1 SM and DM, respectively (bottom), are expressed at equal levels in transfected cells. The intensities of the relevant bands were quantified and normalized to the intensity of the lane with FLAG-p53 alone (indicated as values below the top panel). (D) The PATZ1-p53 interaction inhibits p53 DNA binding to alternative probes (probe 2; derived from the *Gadd45* promoter). (Top and second panels) Precipitation followed by anti-FLAG (top) or anti-HA (second panel) antibody blotting reveals the presence of DNA-bound FLAG-p53 (top, lane 1), and surprisingly, HA-PATZ1 (second panel, lane 2). FLAG-p53 (top, compare lanes 1 and 3) and HA-PATZ1 (second panel, compare lanes 2 and 3) cannot bind to this DNA probe as efficiently in the presence of the other protein. (Third and bottom panels) Lysates of transfected cells show that FLAG-p53 (third panel) and HA-PATZ1 (bottom) are expressed at equal levels in transfected cells. The intensities of the relevant bands were quantified and normalized to the intensity of the lane with FLAG-p53 alone (indicated as values below the top panel). (E) The PATZ1-p53 interaction inhibits PATZ1 DNA binding to PATZ1 probes. (Top and second panels) Precipitation followed by anti-HA (top) or anti-FLAG (second panel) antibody blotting reveals the presence of DNA-bound HA-PATZ1 or HA-PATZ1Alt (top, lanes 1 and 2) but not FLAG-p53 (second panel, lane 3). HA-PATZ1 cannot bind to its probe in the presence of FLAG-p53 as efficiently (top, lane 4). However, the presence of FLAG-p53 does not affect DNA binding of PATZ1Alt (top, lane 5). (Third and bottom panels) Lysates of transfected cells show that FLAG-p53 (bottom) and HA-PATZ1 and HA-PATZ1Alt (third panel) are expressed at equal levels in transfected cells. The intensities of the relevant bands were quantified and normalized to the intensity of the lane with HA-PATZ1 alone (indicated as values below the top panel). (B to E) Biotinylated DNA probes incubated with lysates from HCT116 p53$^{-/-}$ cells transfected with the indicated plasmids were precipitated with streptavidin-conjugated magnetic beads. Pulldown experiments were repeated at least 3 times with independent lysates, and averages of data for the quantitation of the bands observed in Western blots are depicted as bar graphs on the right. Error bars indicate standard errors of the means.
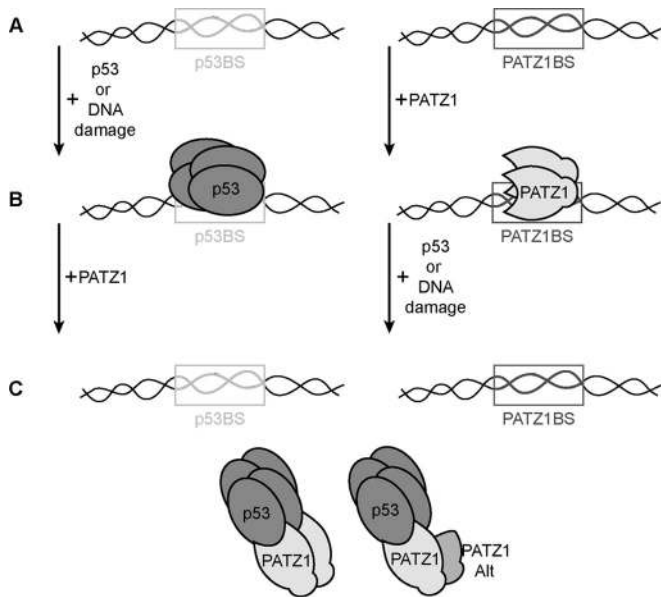
FIG 7 Model for the PATZ1-p53 interaction. p53 and PATZ1 binding sites (boxes labeled p53BS and PATZ1BS, respectively) can be bound by tetrameric p53 (dark gray) after induction of DNA damage or p53 overexpression. PATZ1 proteins (light gray) bind to p53 and inhibit most p53 from binding to DNA. The p53 association can also inhibit the PATZ1 protein from binding the PATZ1 binding site. PATZ1 is a homodimer and can also form heterodimers with the PATZ1Alt variant, which does not directly contact p53. PATZ1 homo- or heterodimerization requires the N-terminal BTB domain.

ACKNOWLEDGMENTS

REFERENCES

1. **Vousden KH, Prives C.** 2009. Blinded by the light: the growing complexity of p53. Cell **137:**413–431. http://dx.doi.org/10.1016/j.cell.2009.04.037.
2. **Levine AJ, Oren M.** 2009. The first 30 years of p53: growing ever more complex. Nat Rev Cancer **9:**749–758. http://dx.doi.org/10.1038/nrc2723.
3. **Marine J-C, Francoz S, Maetens M, Wahl G, Toledo F, Lozano G.** 2006. Keeping p53 in check: essential and synergistic functions of Mdm2 and Mdm4. Cell Death Differ **13:**927–934. http://dx.doi.org/10.1038/sj.cdd.4401912.
4. **El-Deiry W, Kern S, Pietenpol J, Kinzler K, Vogelstein B.** 1992. Definition of a consensus binding site for p53. Nat Genet **1:**45–49. http://dx.doi.org/10.1038/ng0492-45.
5. **Riley T, Sontag E, Chen P, Levine A.** 2008. Transcriptional control of human p53-regulated genes. Nat Rev Mol Cell Biol **9:**402–412. http://dx.doi.org/10.1038/nrm2395.
6. **Wei C-L, Wu Q, Vega VB, Chiu KP, Ng P, Zhang T, Shahab A, Yong HC, Fu Y, Weng Z, Liu J, Zhao XD, Chew J-L, Lee YL, Kuznetsov VA, Sung W-K, Miller LD, Lim B, Liu ET, Yu Q, Ng H-H, Ruan Y.** 2006. A global map of p53 transcription-factor binding sites in the human genome. Cell **124:**207–219. http://dx.doi.org/10.1016/j.cell.2005.10.043.
7. **Li M, He Y, Dubois W, Wu X, Shi J, Huang J.** 2012. Distinct regulatory mechanisms and functions for p53-activated and p53-repressed DNA damage response genes in embryonic stem cells. Mol Cell **46:**30–42. http://dx.doi.org/10.1016/j.molcel.2012.01.020.
8. **Kenzelmann Broz D, Spano Mello S, Bieging KT, Jiang D, Dusek RL, Brady CA, Sidow A, Attardi LD.** 2013. Global genomic profiling reveals an extensive p53-regulated autophagy program contributing to key p53 responses. Genes Dev **27:**1016–1031. http://dx.doi.org/10.1101/gad.212282.112.
9. **Fedele M, Benvenuto G, Pero R, Majello B, Battista S, Lembo F, Vollono E, Day PM, Santoro M, Lania L, Bruni CB, Fusco A, Chiariotti L.** 2000. A novel member of the BTB/POZ family, PATZ, associates with the RNF4 RING finger protein and acts as a transcriptional repressor. J Biol Chem **275:**7894–7901. http://dx.doi.org/10.1074/jbc.275.11.7894.
10. **Costoya JA.** 2007. Functional analysis of the role of POK transcriptional repressors. Brief Funct Genomic Proteomic **6:**8–18. http://dx.doi.org/10.1093/bfgp/elm002.
11. **Siggs O, Beutler B.** 2012. The BTB-ZF transcription factors. Cell Cycle **11:**3358–3369. http://dx.doi.org/10.4161/cc.21277.
12. **Ow JR, Ma H, Jean A, Goh Z, Lee YH, Chong YM, Soong R, Fu X-Y, Yang H, Wu Q.** 2014. Patz1 regulates embryonic stem cell identity. Stem Cells Dev **23:**1062–1073. http://dx.doi.org/10.1089/scd.2013.0430.
13. **Pero R, Palmieri D, Angrisano T, Valentino T, Federico A, Franco R, Lembo F, Klein-Szanto AJ, Del Vecchio L, Montanaro D, Keller S, Arra C, Papadopoulou V, Wagner SD, Croce CM, Fusco A, Chiariotti L, Fedele M.** 2012. POZ-, AT-hook-, and zinc finger-containing protein (PATZ) interacts with human oncogene B cell lymphoma 6 (BCL6) and is required for its negative autoregulation. J Biol Chem **287:**18308–18317. http://dx.doi.org/10.1074/jbc.M112.346270.
14. **Bilic I, Koesters C, Unger B, Sekimata M, Hertweck A, Maschek R, Wilson CB, Ellmeier W.** 2006. Negative regulation of CD8 expression via Cd8 enhancer-mediated recruitment of the zinc finger protein MAZR. Nat Immunol **7:**392–400. http://dx.doi.org/10.1038/ni1311.
15. **Abramova A, Sakaguchi S, Schebesta A, Hassan H, Boucheron N, Valent P, Roers A, Ellmeier W.** 2013. The transcription factor MAZR preferentially acts as a transcriptional repressor in mast cells and plays a minor role in the regulation of effector functions in response to FcεRI stimulation. PLoS One **8:**e77677. http://dx.doi.org/10.1371/journal.pone.0077677.
16. **Sakaguchi S, Hombauer M, Bilic I, Naoe Y, Schebesta A, Taniuchi I, Ellmeier W.** 2010. The zinc-finger protein MAZR is part of the transcription factor network that controls the CD4 versus CD8 lineage fate of double-positive thymocytes. Nat Immunol **11:**442–448. http://dx.doi.org/10.1038/ni.1860.
17. **Valentino T, Palmieri D, Vitiello M, Pierantoni GM, Fusco A, Fedele M.** 2013. PATZ1 interacts with p53 and regulates expression of p53-target genes enhancing apoptosis or cell survival based on the cellular context. Cell Death Dis **4:**e963. http://dx.doi.org/10.1038/cddis.2013.500.
18. **Yang W, Ravatn R, Kudoh K.** 2010. Interaction of the regulatory subunit of the cAMP-dependent protein kinase with PATZ1 (ZNF278). Biochem Biophys Res Commun **391:**1318–1323. http://dx.doi.org/10.1016/j.bbrc.2009.12.026.
19. **Kobayashi A, Yamagiwa H, Hoshino H, Muto A, Sato K, Morita M, Hayashi N, Yamamoto M, Igarashi K.** 2000. A combinatorial code for gene expression generated by transcription factor Bach2 and MAZR (MAZ-related factor) through the BTB/POZ domain. Mol Cell Biol **20:**1733–1746. http://dx.doi.org/10.1128/MCB.20.5.1733-1746.2000.
20. **Mastrangelo T, Modena P, Tornielli S, Bullrich F, Testi MA, Mezzelani A, Radice P, Azzarelli A, Pilotti S, Croce CM, Pierotti MA, Sozzi G.** 2000. A novel zinc finger gene is fused to EWS in small round cell tumor. Oncogene **19:**3799–3804. http://dx.doi.org/10.1038/sj.onc.1203762.
21. **Cho JH, Kim MJ, Kim KJ, Kim J-R.** 2012. POZ/BTB and AT-hook-containing zinc finger protein 1 (PATZ1) inhibits endothelial cell senescence through a p53 dependent pathway. Cell Death Differ **19:**703–712. http://dx.doi.org/10.1038/cdd.2011.142.

22. **Silverstone A, Sun L, Witte ON, Baltimore D.** 1980. Biosynthesis of murine terminal deoxynucleotidyltransferase. J Biol Chem **255:**791–796.

23. **Groves T, Katis P, Madden Z, Manickam K, Ramsden D, Wu G, Guidos CJ.** 1995. In vitro maturation of clonal CD4+CD8+ cell lines in response to TCR engagement. J Immunol **154:**5011–5022.

24. **Naviaux RK, Costanzi E, Haas M, Verma IM.** 1996. The pCL vector system: rapid production of helper-free, high-titer, recombinant retroviruses. J Virol **70:**5701–5705.

25. **Morgenstern JP, Land H.** 1990. Advanced mammalian gene transfer: high titre retroviral vectors with multiple drug selection markers and a complementary helper-free packaging cell line. Nucleic Acids Res **18:**3587–3596. http://dx.doi.org/10.1093/nar/18.12.3587.

26. **El-Deiry W.** 1993. WAF1, a potential mediator of p53 tumor suppression. Cell **75:**817–825. http://dx.doi.org/10.1016/0092-8674(93)90500-P.

27. **Yu J, Zhang L, Hwang PM, Kinzler KW, Vogelstein B.** 2001. PUMA induces the rapid apoptosis of colorectal cancer cells. Mol Cell **7:**673–682. http://dx.doi.org/10.1016/S1097-2765(01)00213-1.

28. **Gibson DG, Young L, Chuang R-Y, Venter JC, Hutchison CA, Smith HO.** 2009. Enzymatic assembly of DNA molecules up to several hundred kilobases. Nat Methods **6:**343–345. http://dx.doi.org/10.1038/nmeth .1318.

29. **Ayed A, Mulder FAA, Yi GS, Lu Y, Kay LE, Arrowsmith CH.** 2001. Latent and active p53 are identical in conformation. Nat Struct Biol **8:**756–760. http://dx.doi.org/10.1038/nsb0901-756.

30. **Schneider CA, Rasband WS, Eliceiri KW.** 2012. NIH Image to ImageJ: 25 years of image analysis. Nat Methods **9:**671–675. http://dx.doi.org/10 .1038/nmeth.2089.

31. **Reich M, Liefeld T, Gould J, Lerner J, Tamayo P, Mesirov JP.** 2006. GenePattern 2.0. Nat Genet **38:**500–501. http://dx.doi.org/10.1038/ng0506-500.

32. **Langmead B, Salzberg SL.** 2012. Fast gapped-read alignment with Bowtie 2. Nat Methods **9:**357–359. http://dx.doi.org/10.1038/nmeth.1923.

33. **Langmead B, Trapnell C, Pop M, Salzberg SL.** 2009. Ultrafast and memory-efficient alignment of short DNA sequences to the human genome. Genome Biol **10:**R25. http://dx.doi.org/10.1186/gb-2009-10-3-r25.

34. **Anders S, Huber W.** 2010. Differential expression analysis for sequence count data. Genome Biol **11:**R106. http://dx.doi.org/10.1186/gb-2010-11 -10-r106.

35. **Valentino T, Palmieri D, Vitiello M, Simeone A, Palma G, Arra C,** **Chieffi P, Chiariotti L, Fusco A, Fedele M.** 2013. Embryonic defects and growth alteration in mice with homozygous disruption of the Patz1 gene. J Cell Physiol **228:**646–653. http://dx.doi.org/10.1002/jcp.24174.

36. **Hermeking H, Lengauer C, Polyak K, He TC, Zhang L, Thiagalingam S, Kinzler KW, Vogelstein B.** 1997. 14-3-3 sigma is a p53-regulated inhibitor of G2/M progression. Mol Cell **1:**3–11. http://dx.doi.org/10.1016 /S1097-2765(00)80002-7.

37. **Stogios PJ, Downs GS, Jauhal JJS, Nandra SK, Privé GG.** 2005. Sequence and structural analysis of BTB domain proteins. Genome Biol **6:**R82. http: //dx.doi.org/10.1186/gb-2005-6-10-r82.

38. **Lai JS, Herr W.** 1992. Ethidium bromide provides a simple tool for identifying genuine DNA-independent protein associations. Proc Natl Acad Sci U S A **89:**6958–6962. http://dx.doi.org/10.1073/pnas.89.15.6958.

39. **Khoury MP, Bourdon J-C.** 2010. The isoforms of the p53 protein. Cold Spring Harb Perspect Biol **2:**a000927. http://dx.doi.org/10.1101 /cshperspect.a000927.

40. **Bilic I, Ellmeier W.** 2007. The role of BTB domain-containing zinc finger proteins in T cell development and function. Immunol Lett **108:**1–9. http: //dx.doi.org/10.1016/j.imlet.2006.09.007.

41. **Pero R, Lembo F, Palmieri EA, Vitiello C, Fedele M, Fusco A, Bruni CB, Chiariotti L.** 2002. PATZ attenuates the RNF4-mediated enhancement of androgen receptor-dependent transcription. J Biol Chem **277:**3280–3285. http://dx.doi.org/10.1074/jbc.M109491200.

42. **Shi X, Kachirskaia I, Yamaguchi H, West LE, Wen H, Wang EW, Dutta S, Appella E, Gozani O.** 2007. Modulation of p53 function by SET8-mediated methylation at lysine 382. Mol Cell **27:**636–646. http://dx.doi .org/10.1016/j.molcel.2007.07.012.

43. **Kachirskaia I, Shi X, Yamaguchi H, Tanoue K, Wen H, Wang EW, Appella E, Gozani O.** 2008. Role for 53BP1 Tudor domain recognition of p53 dimethylated at lysine 382 in DNA damage signaling. J Biol Chem **283:**34660–34666. http://dx.doi.org/10.1074/jbc.M806020200.

44. **Botuyan MV, Lee J, Ward IM, Kim J-E, Thompson JR, Chen J, Mer G.** 2006. Structural basis for the methylation state-specific recognition of histone H4-K20 by 53BP1 and Crb2 in DNA repair. Cell **127:**1361–1373. http://dx.doi.org/10.1016/j.cell.2006.10.043.

45. **Huang DW, Sherman BT, Lempicki RA.** 2009. Systematic and integrative analysis of large gene lists using DAVID bioinformatics resources. Nat Protoc **4:**44–57. http://dx.doi.org/10.1038/nprot.2008.211.